Jurnal Mekanikal
Disember 2003, Bil. 16, 47 - 56

EXPERIMENTAL INVESTIGATION OF INCOMPRESSIBLE FLOW AROUND THREE-ELEMENT AIRFOIL AT HIGH ANGLE OF ATTACK

Ashraf A. Omar
Department of Mechanical Engineering
Faculty of Engineering
International Islamic University Malaysia
aao@iiu.edu.my

Tang Chun Chong
Tan Soo Min
Department of Aerospace Engineering
Faculty of Engineering
University Putra Malaysia

ABSTRACT

The experimental investigation of the incompressible flow around a three element airfoil was carried out to study the effect of angle of attack and Reynolds number. The work started with designing, fabricating and testing the multi-element airfoil in the UPM low speed wind tunnel. The results of the experiment were studied in terms of the coefficient of pressure. The results show delay in flow separation and continuity in pressure distribution for studied angles of attack and Reynolds numbers. The performance of multi-element airfoil was compared to a single element airfoil.

Keywords: *Three element airfoil, wind tunnel, coefficient of pressure, angle of attack, Reynolds number*

1.0 INTRODUCTION

The goal of a high-lift system is to generate as much lift as possible without separating the flow. Without external devices such as wall suction, the most effective way to achieve this goal is through the use of multi-element airfoil. Additionally, improvement made in the design of the cruise wings also impacts the design of high-lift system. Therefore, the understanding of and the ability to analyze these element of high lift systems are problems that must be solved in order to allow the aircraft designer to develop a high-lift system which meets the required performance levels.

A great body of work on high-lift flows, both experimental and computational, has been built up in the last few years [3, 4, 6, 8]. Some experiments have been performed solely for the purpose of CFD code validation [4, 6, 8]. There have been many CFD results reported for 2-D multi-element airfoils, using a variety of

schemes for the Euler and Navier-Stokes equations. Structured grid and the unstructured grid have also been applied to 2-D multi-element airfoil.

The complex geometries produced complex viscous flows at most flight conditions. The low speed designer has the task of analyzing this airfoil over a large range of angle of attack. Many of the flow phenomena found on multi-element airfoils are presently not well understood, in particular, those associated with the physics of shear layers, separated flows, boundary layer transition and the effects of gaps and angle of the slat and the flap with the main element. In the past several years, there have been few two-dimensional data published about the effect of high angle of attack and Reynolds number on high lift airfoils.

The primary objective of the current experiment was to investigate the pressure distribution at various angles of attack and a wide range of Reynolds numbers. The important tasks ahead that will be undertaken are to select a suitable multi-element airfoil, fabrication of the model for experimental work, experimental investigation to obtain important parameters, the coefficient of pressure, C_p, verification and analysis of results.

2.0 EXPERIMENTAL WORK

2.1 Designing and fabrication of model

The model is basically based on the McDonnell-Douglas Aerospace three-element airfoil [8] as shown in Figure 1a. The total chord length of the experimental model was selected to be 0.67 m. This selection was based on the dimension of the wind tunnel test section. Details of the model dimension can be seen in Figure 1a in terms of the chord. The slat and flap gap sizes were selected to be 0.02 and 0.027 m, respectively and the slat and flap hanging angles were set to 25 and 30 degrees, respectively.

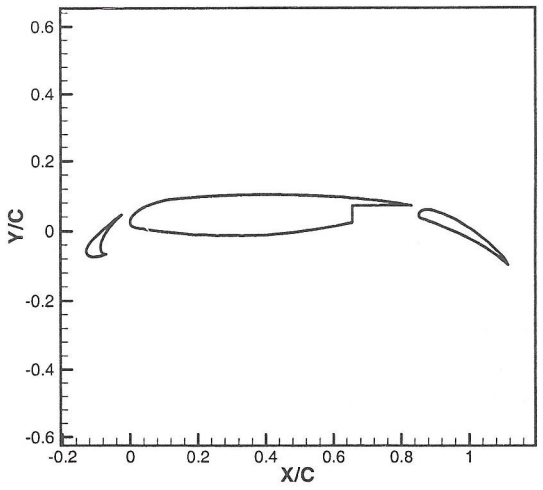

Figure 1a Three element airfoil configuration [8]

The model was designed to enable the slat and flap to be adjustable and extendable. A simple moveable arm was designed to attach the slat and flap to the main elements as shown in Figure 1b.

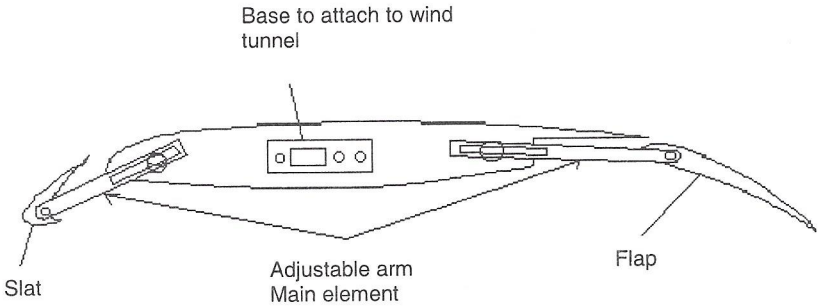

Figure 1b Model fabricated based on the drawing

For the model, plywood was used as the main frame. This decision can be justified because of the characteristics of wood, which is easy to be formed into shape, strong and does not crack easily, with economical cost. In order to get the exact shape as in the drawing, the frame was constantly checked with the drawing in order to detect any defect before skinning. For the skin of the model, aluminum 2024-T3 with thickness of approximately one *mm* was used. This will naturally give a smooth surface to the model and ease forming into shape. In order to reduce the roughness of the surface, glue was used to attach the skin to the frame. A few layers of coating were applied on the surface to get a better smoothness.

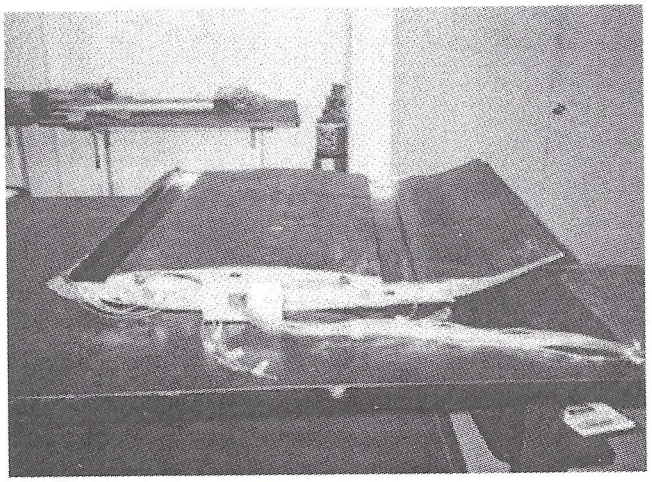

Figure 2 Experimental model

For the pressure tapping points, there were 44 chordwise points on the model. The fabricated model has 7 points on the slat, 25 points on the main element and 12 points on the flap. Due to the limitation of space, the number of points were only 44. The locations of the pressure tapping points on the experimental model are presented in Table 1.

For easy fitting and adjustability, the base of the model was made from plastic. The experimental model is shown in Figure 2.

2.2 Experiment and evaluation of model

The experiments were carried out in an open loop low speed wind tunnel in the aerodynamic laboratory, Universiti Putra Malaysia (Figure 3). The test section dimensions are 1×1×2.5 m. The flow velocity can be adjusted and velocities up to 50 m/s can be reached.

Before running the experiment, the model had undergone a test using the wind tunnel to identify the pressure tapping points that are not working properly. Testing the model for a few configurations and speeds gave a good overview of the experimental procedures.

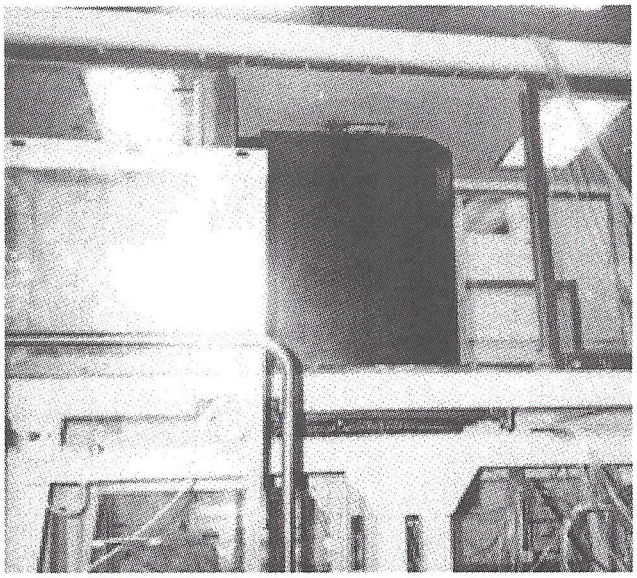

Figure 3 Experimental model airfoil mounted in UPM Aero Lab open loop low speed wind tunnel test section

To avoid strong vibration at high speeds or high angle of attacks and to make sure that the results were acceptable, a few test cases were carried out to set up limiting speeds and angles of attack. This will help in eliminating error due to structural intolerance to experimental conditions. The results from the experiment were divided into 32 groups of combinations that will be evaluated. Each of the configurations was tested with three different speeds to study the differences and consistencies of the results in order to detect any error in reading early. By

constantly cross checking the results, the error of getting an ambiguous reading can be reduced.

Evaluation of the experimental results was done through out the process and cross-reference was done with the theoretical prediction and results from previous published experiments [3, 6]. This was done to detect any error so that experiment on the configuration can be repeated.

2.3 Run Procedures

The following procedures are followed during the model testing in the wind tunnel:

1) Multi-element airfoil is installed into the wind-tunnel test section.
2) All the tubes for the pressure tapping points are connected to pressure gauge (manometer).
3) Angles of slat, flap and main element are fixed.
4) Gap sizes for slat and flap are fixed.
5) Angles of attack are selected.
6) Wind tunnel is operated at the speed of 10m/s.
7) Readings of the pressure gauge are recorded.
8) Steps 5 and 6 are repeated for speeds of 18m/s and 23m/s.
9) Steps 5 to 7 are repeated for different wind tunnel speeds.

2.4 Presentation of the Results

The most critical part of the experiment is the analysis of the results in order to understand the interactions, usage and effects of the elements on the overall flow pattern. In order to give a better picture of the flow patterns around the multi-element airfoil, the results are tabulated and manipulated into the form of coefficient of pressure. To give a better perspective of pressure distribution and aerodynamic forces on the elements, the graphs are divided into two sections comprising of upper and lower surface.

The analysis of the experimental results is more towards interactions and effects of the elements on the flow distribution patterns. Multi-element airfoil plays an important role as passive devices to manipulate inviscid pressure distribution to reduce pressure rise over each element, to avoid severe adverse pressure gradient and flow separation without the usage of external devices such as wall suction.

Results are presented as coefficient of pressure on the surfaces of the three elements (Slat, Main and Flap). Below are the constants used for the experiment:

Air density, $\rho_\infty = 1.01325 \frac{kg}{m^3}$ Gravitational acceleration, $g = 9.81 \frac{m}{s^2}$

Water density, $\rho_w = 1000 \frac{kg}{m^3}$

2.5 Coefficient of pressure, C_p

The calculation method used in finding the value of coefficient of pressure, C_p is as follows:

$$C_p = \frac{P - P_\infty}{\frac{1}{2}\rho_\infty V^2} \tag{1}$$

By substituting $P = P_\infty - \Delta l \rho_w g$ into Equation (1), the following relation can be obtained:

$$C_P = \frac{-\Delta l \rho_w g}{\frac{1}{2}\rho_\infty V^2} \tag{2}$$

The graphs of coefficient of pressure, C_p along the chord length show the chordwise pressure distribution and the interaction between the elements and the respective flow. Analysis of the results is based on the patterns observed from the graphs and its significance for application.

3.0 RESULTS AND DISCUSSION

As shown in Figure 4a to Figure 4c, when the Reynolds number increases, the differences in the value of C_p between the upper and lower surfaces increases. The increase in magnitude is predictable because increases in Reynolds number will increase the pressure force acting on the airfoil. Examination of the pressure distribution at the leading edge of the main airfoil and flap clearly shows region of flow separation. This separation region between the elements will help minimize the effects of wake from the previous element to the latter that might alter its flow pattern and meeting of weak wake with severe adverse pressure gradient might cause flow reversal about the leading edge.

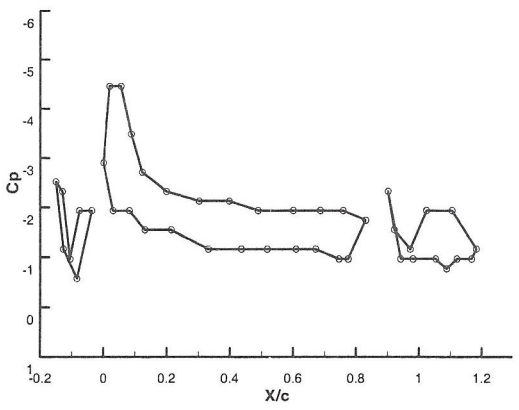

(a) $R_{e_c} = 0.45 \times 10^6$

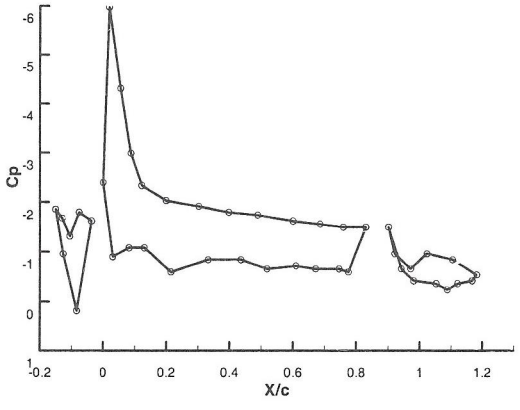

(b) $R_{e_c} = 0.8 \times 10^6$

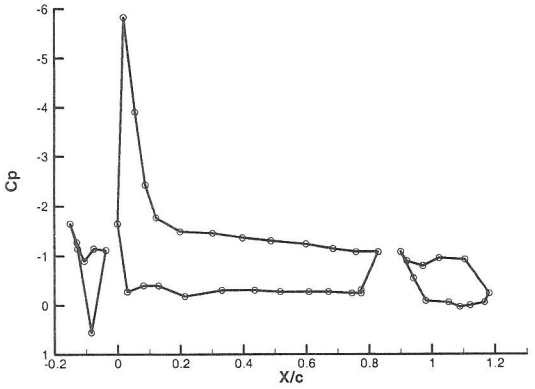

(c) $R_{e_c} = 1.12 \times 10^6$

Figure 4 Distribution of surface-pressure coefficient at various Reynolds number ($\alpha = 10°$)

The effects of increasing the angle of attack can be seen in Figure 5, where pressure differences between the upper and lower surfaces are higher at $\alpha = 23.3°$ when compared to $\alpha = 10°$. This happens mainly due to the increase in flow speed on the upper surface as compared to the lower surface, hence creating a higher-pressure ratio between the lower and upper surfaces. However, this pattern of increment only persists until a certain angle of attack when the pattern begins to reverse in the opposite direction.

When the angle of attack is set to a negative value (Figure 5c and Figure 5d), the distribution of pressure is in the opposite direction to the pressure distribution when angle of attack is in the positive region. This is due to the formation of negative camber that will reverse the pattern of pressure distribution which creates a high-pressure region on the upper surface compared to the lower surface. Negative lift is observed at this configuration.

For configurations within the region of negative angle of attack, another important phenomenon occurs. Flow separation at the lower surface of flap occurs as suspected at location close to x/c = 1.1. This is due to a sharp increase of the value of C_p followed by a sudden drop in the value of C_p which indicates that the flow accelerated again further downstream and the flow reattaches to the element in this region.

Interaction between elements shows a favourable pattern for almost all the results from the experiment. Delay in flow separation and continuity in pressure distribution are the most important characteristics that make the application of multi-element airfoil feasible. The slotted regions between elements act as a suction point to accelerate the flow around this region, which delay flow separation from the trailing edge of the elements. Interaction between the

elements also reduces the severity of adverse flow at the leading edge of the elements as observed from the graphs (Figures 4 and 5).

In Figure 6, a comparison is made between the results obtained from the present experiment of multi-element airfoil with normal single element airfoil [5]. For a well designed multi-element with sufficient separation between elements, there is no flow separation and reversal which gives a smooth continuous chordwise flow characteristic. For a single element airfoil, flow reversal is observed at the trailing edge of the airfoil. This is due to circulation of flow about this region. 'Tired' flow about the trailing edge is one of the main contributors towards flow reversal.

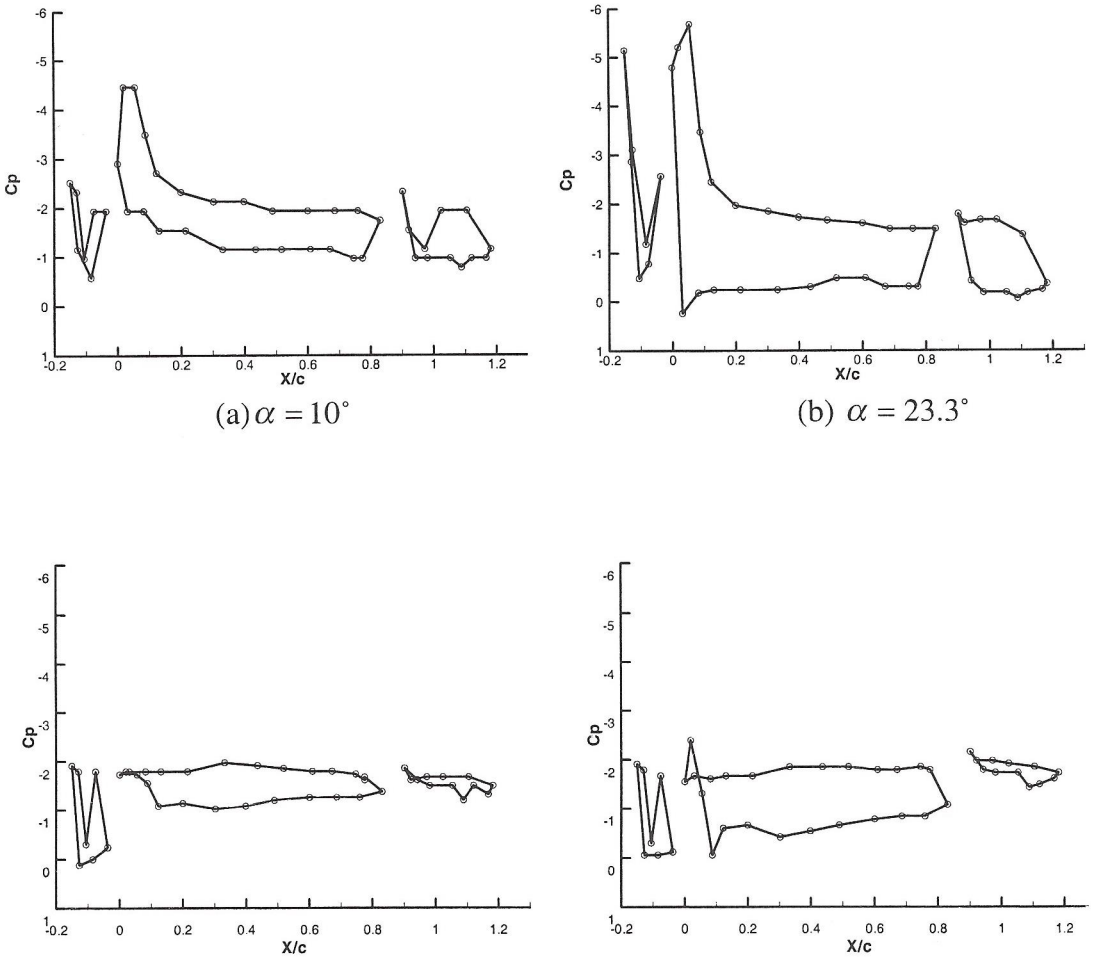

Figure 5 Distribution of surface-pressure coefficient at various angle of attack ($Re_c = 0.45x10^6$)

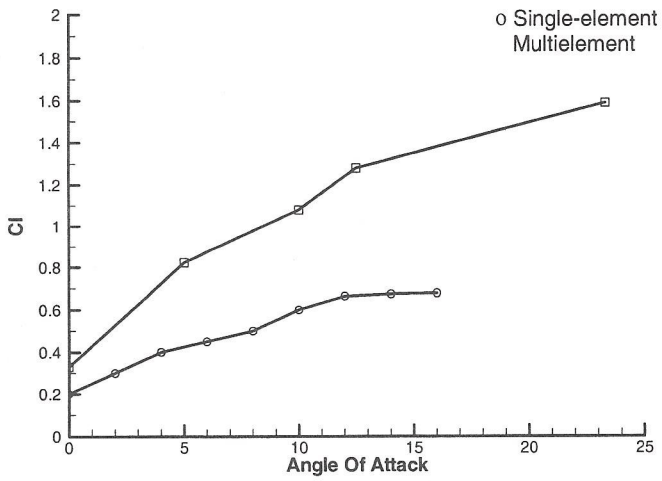

Figure 6 Comparison of C_L vs α between Single-element and Multi-element ($Re_c = 0.25x10^6$).

4.0 CONCLUSIONS

The pressure distributions show the important characteristics for a given three element airfoil. The reduction in severity of adverse pressure gradient has resulted in the reduction of the possibility of flow reversal to occur. Flow reversal will eliminate all the advantages gained by using multi-element airfoil and at the same time increases stall angle. Higher lift is obtained with the use of multi-element airfoil in comparison with the single element airfoil. With the increase of effective angle of attack and Reynolds number, the difference of the value of C_p between the upper and the lower surfaces increases. Therefore, the lift on the multi-element airfoil will increase accordingly.

From the established flow characteristics obtained from the experimental results, the advantages of multi-element airfoil in reducing the severity of adverse pressure gradient, delay flow separation and reduce the possibility of flow reversal are evident. However, there are a few configurations that go against these characteristics. This is mainly due to insufficient separation where the configurations are beyond the optimum configuration which causes the reverse trend to occur.

ACKNOWLEDGEMENT

The authors would like to acknowledge the support of the Ministry of Science, Technology and Environment, Malaysia under the grant No. 09-02-04-0433-EA001. In addition, the authors also like to convey special thanks and gratitude to Associate Professor Dr. Waqar Asrar for his fruitful discussion and help.

REFERENCES

1. Kuethe, A. M. and Chow, C. Y., 1998, "*Foundation of Aerodynamics*", Fifth Edition, John Wiley & Sons, Inc.
2. Anderson, J. D., 1999, " *Aircraft Performance & Design*", WCB/McGraw-Hill.
3. Lim, J. C. and Dominik, C. J., "*Parametric Investigation of a High-lift Airfoil at High Reynolds numbers*", NASA Langley Research Center, Hampton, USA.
4. Rumsey, C. L. and Gatski, T. B., August 2000, "*Recent Turbulence Model Advances Applied to Multielement Airfoil Computations*", 18th Applied Aerodynamics Meeting, NASA Langley Research Center, Hampton, USA, .
5. James, H. A. and Maki, R. L., July 1957, "*Wind-tunnel test of the static longitudinal characteristic at low-speed of a swept-wing airplane with blowing flaps and leading edge slats*", Research Memorandum, Langley Aeronautical Laboratory Library, NACA.
6. Anderson, J. D., "*Navier-Stokes Computations & Experimental Comparisons for Multielement Airfoil Configurations*", NASA Langley Research Center Hampton, USA.
7. Henne, P. A., 1990, "*Applied Computational Aerodynamics*", American Institute of Aeronautics and Astronautics, Inc. Washington D.C.
8. Klausmeyer, S. M., and Lin J. C., May 1997, "*Comparative results from a CFD challenge over a 2D Three-element High-lift Airfoil*", NASA Technical Memorandom 112858.

Table1 Location of pressure tapping points

Tube no.	Position	
	Location	X/C
1	Slat 1	-0.0373
2	2	-0.0843
3	3	-0.1269
4	4	-0.1507
5	5	-0.1299
6	6	-0.1060
7	7	-0.0761
8	Main 1	0.8299
9	2	0.7590
10	3	0.6858
11	4	0.6000
12	5	0.4888
13	6	0.3978
14	7	0.3022
15	8	0.1993
16	9	0.1224
17	10	0.0881
18	11	0.0552
19	12	0.0194
20	13	0.0000
21	14	0.0306
22	15	0.0821

Tube no.	Position	
	Location	X/C
23	16	0.1306
24	17	0.2142
25	18	0.3313
26	19	0.4358
27	20	0.5179
28	21	0.6090
29	22	0.6709
30	23	0.7455
31	24	0.7746
32	25	0.7746
33	Flap 1	1.1821
34	2	1.1052
35	3	1.0231
36	4	0.9716
37	5	0.9209
38	6	0.9015
39	7	0.9418
40	8	0.9806
41	9	1.0530
42	10	1.0881
43	11	1.1209
44	12	1.1672